

SCIENTIFIC REPORTS

OPEN

Nitrous Oxide Production in Co- Versus Counter-Diffusion Nitrifying Biofilms

Lai Peng^{1,2}, Jing Sun¹, Yiwen Liu³, Xiaohu Dai¹ & Bing-Jie Ni¹

Received: 05 April 2016

Accepted: 08 June 2016

Published: 29 June 2016

For the application of biofilm processes, a better understanding of nitrous oxide (N_2O) formation within the biofilm is essential for design and operation of biofilm reactors with minimized N_2O emissions. In this work, a previously established N_2O model incorporating both ammonia oxidizing bacteria (AOB) denitrification and hydroxylamine (NH_2OH) oxidation pathways is applied in two structurally different biofilm systems to assess the effects of co- and counter-diffusion on N_2O production. It is demonstrated that the diffusion of NH_2OH and oxygen within both types of biofilms would form an anoxic layer with the presence of NH_2OH and nitrite (NO_2^-), which would result in a high N_2O production via AOB denitrification pathway. As a result, AOB denitrification pathway is dominant over NH_2OH oxidation pathway within the co- and counter-diffusion biofilms. In comparison, the co-diffusion biofilm may generate substantially higher N_2O than the counter-diffusion biofilm due to the higher accumulation of NH_2OH in co-diffusion biofilm, especially under the condition of high-strength ammonium influent (500 mg N/L), thick biofilm depth (300 μm) and moderate oxygen loading ($\sim 1\text{--}4 \text{ m}^3/\text{d}$). The effect of co- and counter-diffusion on N_2O production from the AOB biofilm is minimal when treating low-strength nitrogenous wastewater.

The destruction of stratospheric ozone layer has become a significant environmental issue in 21st century, which is contributed largely by nitrous oxide (N_2O)¹. According to IPCC², the N_2O concentration in global atmosphere has increased from pre-industrial value of around 271 ppbv to 324 ppbv in 2011 due to human activities comprising agriculture, industry, fossil fuel combustion, and wastewater treatment. N_2O is also a potent greenhouse gas with a global warming potential (GWP) of approximately 265 times stronger than carbon dioxide². In terms of this, even a low emission of N_2O from wastewater treatment is environmental hazardous and thus unwanted.

Ammonia oxidizing bacteria (AOB) have been recognized as the main contributor to N_2O production from wastewater treatment plants (WWTPs)^{3–6}. It is commonly believed that N_2O is generated by AOB via two pathways: the first involves sequential reductions from nitrite (NO_2^-) to nitric oxide (NO) and from NO to N_2O as the end product, termed as AOB denitrification pathway^{4,7–9}; the second includes incomplete oxidation of hydroxylamine (NH_2OH) with N_2O as the side product, known as NH_2OH oxidation pathway^{8,10,11}. The AOB denitrification pathway is favored at oxygen (O_2) limiting conditions with nitrite accumulation^{4,7,12}, whilst the NH_2OH oxidation pathway is significantly promoted by elevated oxygen concentration^{8,13}. Therefore, the varying DO and nitrite concentrations may trigger the shift of the two known N_2O pathways^{6,14}.

To reveal the mechanism of N_2O production by AOB and enhance our ability to predict site-specific N_2O production in WWTPs, Ni *et al.*¹⁵ developed an integrated N_2O model incorporating both AOB denitrification and NH_2OH oxidation pathways. Electron mediators (Mred as the reduced form and Mox as the oxidized form) were used to model the electron transfer from oxidation to reduction in biochemical reactions. This two-pathway model has been evaluated using the experimental data from several highly different cultures performing nitrification and/or nitrification, respectively and successfully applied for prediction of N_2O production from a step-feed full-scale wastewater treatment reactor^{15,16}.

There is a rapid development and growing utilization of biofilm processes (e.g. membrane biofilm reactors, fluidized bed reactors, rotating biological contractors, granular biofilter, trickling filters etc.) during wastewater

¹State Key Laboratory of Pollution Control and Resources Reuse, College of Environmental Science and Engineering, Tongji University, Shanghai 200092, PR China. ²Laboratory of Microbial Ecology and Technology (LabMET), Ghent University, Coupure Links 653, Ghent 9000, Belgium. ³Centre for Technology in Water and Wastewater, School of Civil and Environmental Engineering, University of Technology Sydney, Sydney, 2007 NSW, Australia. Correspondence and requests for materials should be addressed to B.-J.N. (email: bjni@tongji.edu.cn)

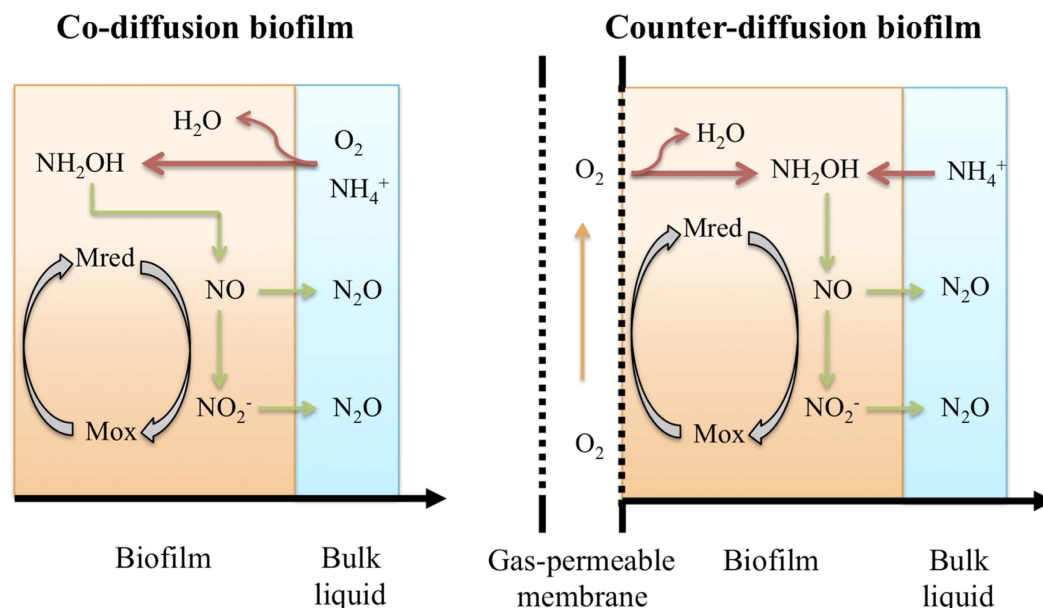


Figure 1. A simplified scheme of the co- (left) and counter-diffusion (right) biofilm structure with the two different N_2O production pathways by AOB in nitrifying biofilms.

treatment. Different from the suspended-growth sludge, N_2O production from the biofilm may be affected by the stratification of electron donors, acceptors and microbes. For example, based on mathematical modeling, Sabba *et al.*¹⁷ observed that the diffusion of NH_2OH from aerobic region to anoxic region would result in a substantially higher N_2O production in biofilm than that in suspended-growth sludge.

In conventional biofilm systems, all of the substrates are supplied into the biofilm from the bulk liquid, while in membrane aerated biofilm reactors (MABR), the oxygen and other substrates are dividedly provided to the biofilm base through a gas-permeable membrane and surface of the biofilm from the bulk liquid, respectively (Fig. 1). The former is known as the co-diffusion biofilm and the latter is termed as the counter-diffusion biofilm^{18,19}. This work aims to reveal the key difference of N_2O production from the co- versus counter-diffusion nitrifying biofilms and the associated underlying mechanisms of N_2O production by AOB from the co- and counter-diffusion biofilms using the two-pathway N_2O ¹⁵.

Results

The effect of co- and counter-diffusion on N_2O production from AOB biofilms at varying bio-film thicknesses and oxygen loadings. Figure 2 illustrates the simulation results using the two-pathway model in both co- and counter-diffusion biofilms with different biofilm thicknesses and oxygen loading rates applied. Since there is no gas stripping process in bulk liquid, the effluent N_2O concentration could be considered as the total N_2O production by the AOB biofilm. For both diffusion geometries with biofilm thickness of $100\ \mu\text{m}$ (Fig. 2A), the effluent N_2O concentrations increased as oxygen loading increased initially, reached the peak at oxygen loading of approximately $4.5\ \text{m}^3/\text{d}$ and slightly decreased after oxygen loading further increased to $5.5\ \text{m}^3/\text{d}$. N_2O productions from the co-diffusion and counter-diffusion biofilms were similar at most oxygen loadings, except the ones between $\sim 1.2\sim 2.8\ \text{m}^3/\text{d}$, where N_2O production from the co-diffusion biofilm was slightly higher than that from the counter-diffusion biofilm (Fig. 2A).

Figure 2B presents the effluent N_2O concentration of the co- and counter-diffusion AOB biofilms with biofilm thickness of $200\ \mu\text{m}$. The maximum effluent N_2O concentration was obtained at oxygen loading of approximately $4.25\ \text{m}^3/\text{d}$ for both co- and counter-diffusion biofilms. With the further increase or decrease of oxygen loading, a lower effluent N_2O concentration was observed. The N_2O production at biofilm thickness of $200\ \mu\text{m}$ (Fig. 2B) was much higher than that from thinner biofilm (Fig. 2A). In the oxygen loading ranges of $\sim 0.8\sim 2.4\ \text{m}^3/\text{d}$ and $\sim 3.5\sim 5\ \text{m}^3/\text{d}$, the N_2O production from the co-diffusion biofilm was higher than that from counter-diffusion biofilm (Fig. 2B).

In Fig. 2C, for counter-diffusion biofilm, the increase of biofilm thickness from 200 to $300\ \mu\text{m}$ didn't alter the overall trend of effluent N_2O concentration against increasing oxygen loading, but rather led to a minor elevated overall N_2O production. However, the effluent N_2O concentration in the co-diffusion biofilm with $300\ \mu\text{m}$ biofilm thickness (Fig. 2C) peaked at oxygen loading of around $2.4\ \text{m}^3/\text{d}$. By comparing N_2O production from the co-diffusion biofilm with that from the counter-diffusion biofilm, it has been found: within oxygen loading of 0.24 to $\sim 1\ \text{m}^3/\text{d}$, the N_2O productions from both diffusion geometries were similar to each other; in the range of $\sim 1\sim 4\ \text{m}^3/\text{d}$, the N_2O production from the co-diffusion biofilm was substantially higher than that from the counter-diffusion biofilm; With the increase of the oxygen loading from $\sim 4\sim 5.5\ \text{m}^3/\text{d}$, the counter-diffusion biofilm produced more N_2O (Fig. 2C).

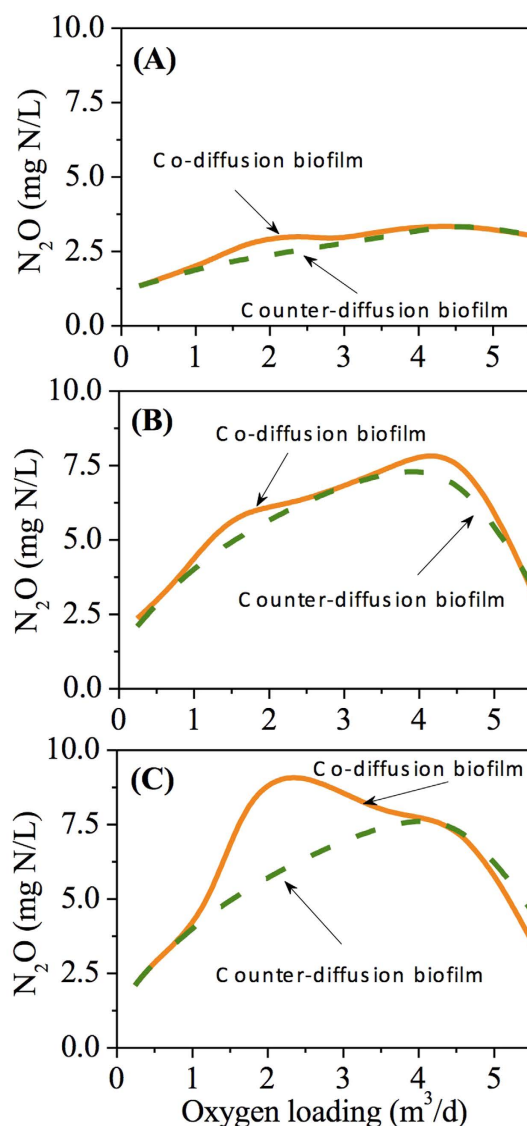


Figure 2. The effluent N_2O concentrations from co- and counter-diffusion biofilm reactors as a function of oxygen loading with varying biofilm thicknesses applied: (A) $100\ \mu\text{m}$; (B) $200\ \mu\text{m}$; and (C) $300\ \mu\text{m}$. (The applied influent ammonium concentration and HRT are $500\ \text{mg N/L}$ and $12\ \text{h}$, respectively).

To further identify the N_2O source under the tested simulation conditions of Fig. 2C, the relative contributions of AOB denitrification pathway and NH_2OH oxidation pathway to N_2O production in AOB biofilm are illustrated in Figure S1 in Supplementary Material. For both diffusion geometries, the contribution of AOB denitrification pathway decreased with the increase of oxygen loading, accompanied by a corresponding increase of the contribution of NH_2OH oxidation pathway. AOB denitrification pathway served to be the major contributor to N_2O production (over 90% for all cases).

Analysis of N_2O production within the co- and counter- diffusion nitrifying biofilms at low oxygen loading ($0.24\ \text{m}^3/\text{d}$). To reveal the mechanisms leading to the variation between N_2O production from the co-diffusion biofilm and from the counter-diffusion biofilm, the simulation results of depth profiles with biofilm thickness of $300\ \mu\text{m}$ at oxygen loadings of 0.24 , 2.4 and $5.5\ \text{m}^3/\text{d}$ (see Fig. 2C) are presented in Figs 3–5.

In Fig. 3, with an influent ammonium concentration of $500\ \text{mg N/L}$, HRT of $12\ \text{h}$ and oxygen supply of $0.24\ \text{m}^3/\text{d}$, the distribution of O_2 , NH_2OH , Mox , Mred and N_2O production rate via the two known pathways throughout the biofilm are depicted. The effluent concentration of NH_4^+ and NO_2^- of the AOB biofilm for both diffusion geometries were ~ 470 and $\sim 27\ \text{mg N/L}$, respectively as shown in Figure S2 in Supplementary Material. The concentration of NH_4^+ and NO_2^- were relatively constant within the biofilm and close to the effluent concentrations (data not shown).

In the co-diffusion biofilm, the O_2 concentration was $\sim 0.055\ \text{mg O}_2/\text{L}$ at the outer layer of the biofilm, decreased gradually towards the base of biofilm and was depleted at a biofilm thickness of $\sim 200\ \mu\text{m}$ (Fig. 3A). The NH_2OH concentration within the biofilm displayed a similar trend against biofilm depth and completely depleted

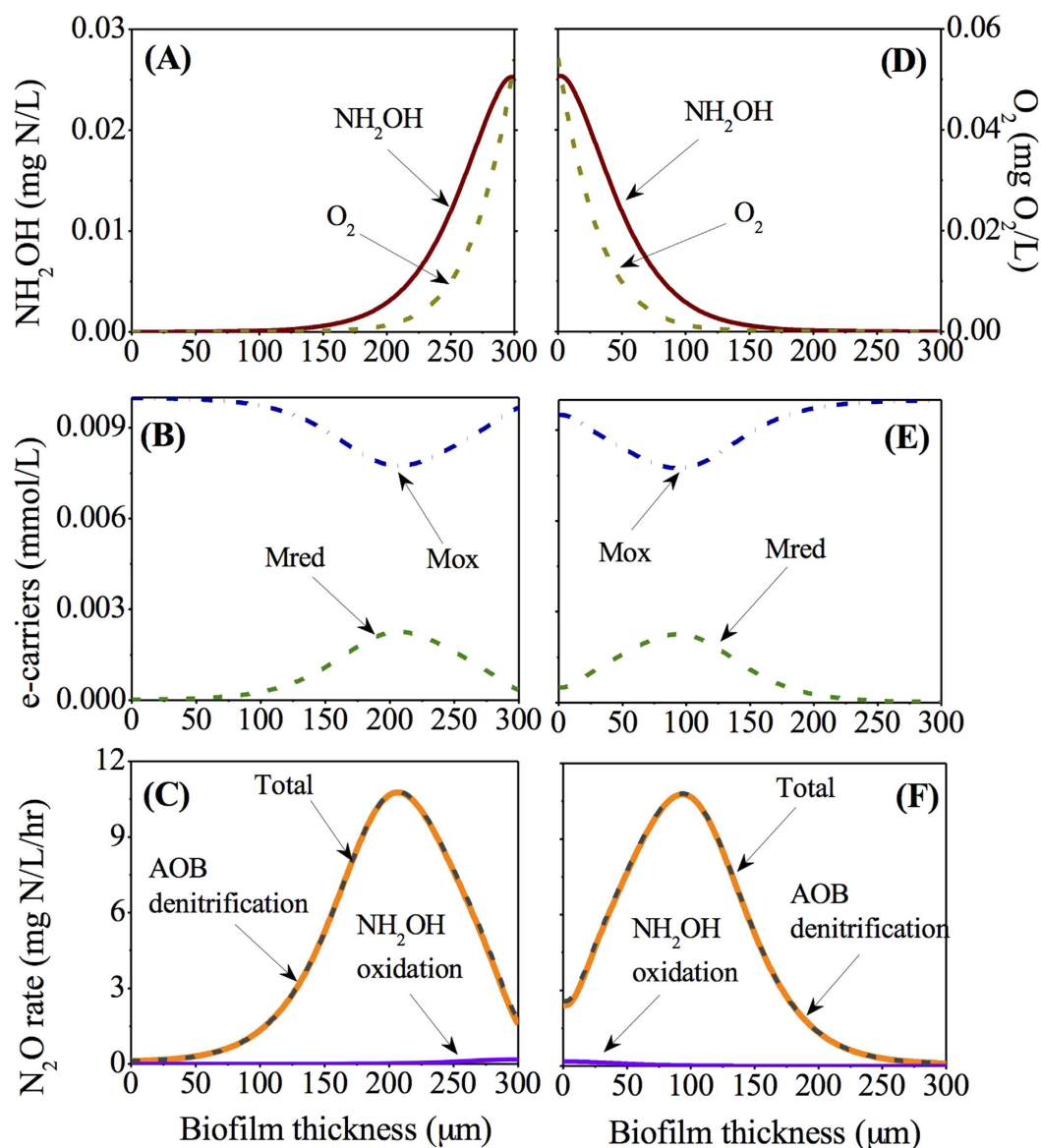


Figure 3. The depth profiles of NH_2OH , O_2 , Mred, Mox and N_2O production rates at low oxygen loading ($0.24 \text{ m}^3/\text{d}$) within the co-diffusion biofilm (A–C) and counter-diffusion biofilm (D–F).

at a biofilm depth of $\sim 150 \mu\text{m}$ (Fig. 3A). The Mred concentration peaked at a biofilm thickness of $\sim 200 \mu\text{m}$, where the Mox concentration was minimal (Fig. 3B). The distribution of N_2O production rate matches the predicted Mred stratification of the biofilm with negligible contribution from NH_2OH oxidation pathway (Fig. 3C).

An opposite distribution profile is observed in the counter-diffusion biofilm. The concentration of O_2 and NH_2OH were maximal at the base of biofilm, decreased as biofilm thickness increased and was depleted at $100 \mu\text{m}$ and $150 \mu\text{m}$, respectively (Fig. 3D). The highest point of Mred and lowest point of Mox were observed at a biofilm depth of $100 \mu\text{m}$ (Fig. 3E). The N_2O production rate was also in good agreement with the Mred distribution profiles, which was mostly contributed by AOB denitrification pathway (Fig. 3F). The average concentrations of O_2 , NH_2OH , Mred and Mox as well as the average N_2O production rate, despite the varying distribution within the biofilm, were very similar in the co-diffusion and counter-diffusion biofilms, resulting in the similar N_2O production in co- and counter diffusion biofilms under such low oxygen loading (Fig. 2C).

Analysis of N_2O production within the co- and counter- diffusion nitrifying biofilms at moderate oxygen loading ($2.4 \text{ m}^3/\text{d}$). Figure 4 shows the stratification profiles of O_2 , NH_2OH , Mox, Mred and N_2O production rate via the two known pathways within the biofilms, with an influent ammonium concentration of 500 mg N/L , HRT of 12 hours and oxygen supply of $2.4 \text{ m}^3/\text{d}$. The concentration of NH_4^+ and NO_2^- in effluent (Figure S2) and within the AOB biofilm for both diffusion geometries were in the ranges of $\sim 222\text{--}\sim 228 \text{ mg N/L}$ and $\sim 258\text{--}\sim 260 \text{ mg N/L}$, respectively.

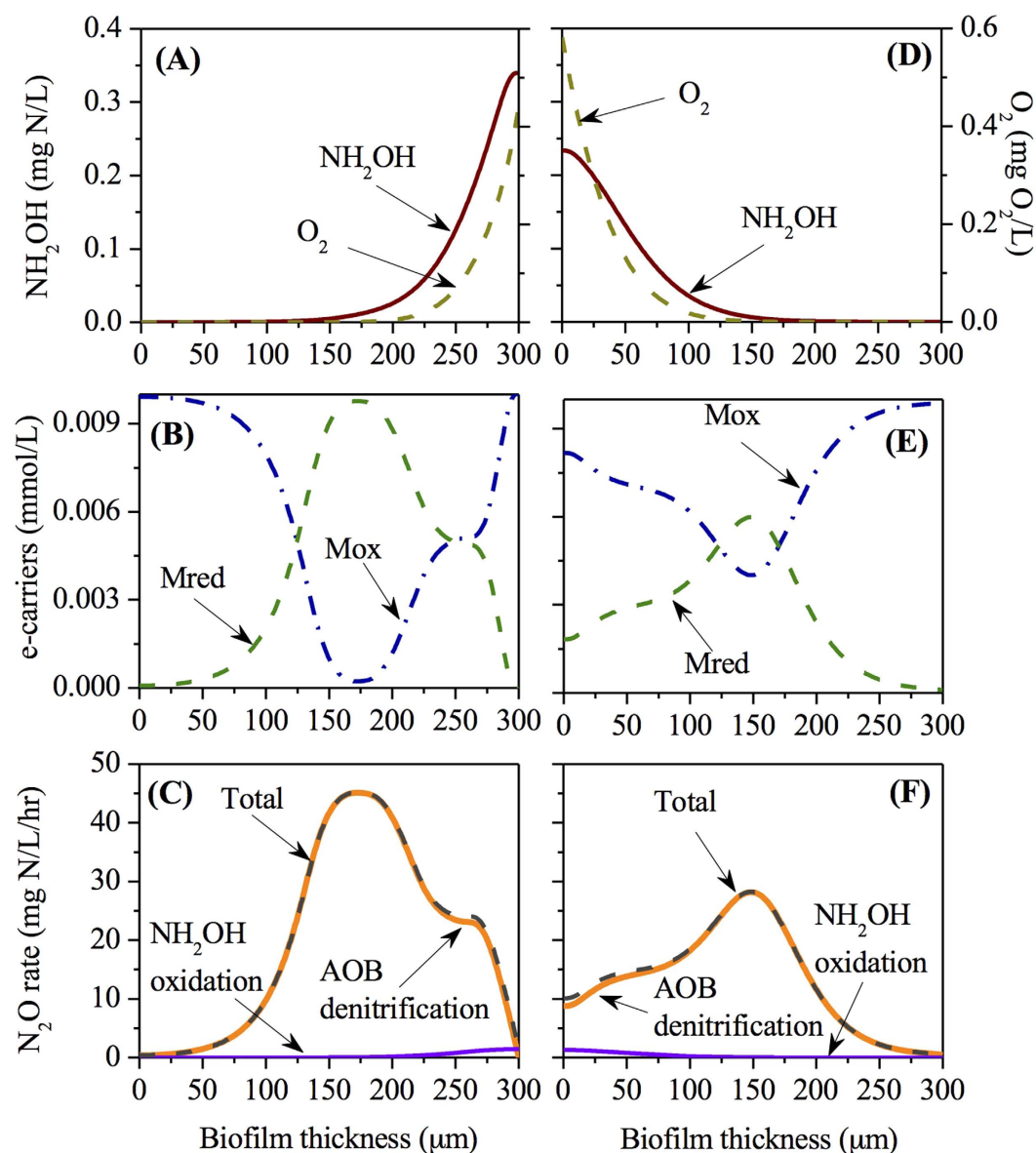


Figure 4. The depth profiles of NH_2OH , O_2 , Mred , Mox and N_2O production rates at moderate oxygen loading ($2.4 \text{ m}^3/\text{d}$) within the co-diffusion biofilm (A–C) and counter-diffusion biofilm (D–F).

The distribution profiles of O_2 and NH_2OH in the co-diffusion biofilm were opposite to those in the counter-diffusion biofilm. The O_2 and NH_2OH within the biofilm decreased from the surface to the base and were depleted at 200 μm and 150 μm , respectively in the co-diffusion biofilm, while their concentrations decreased from base to surface and were depleted at 125 μm and 150 μm , respectively in the counter-diffusion biofilm (Fig. 4A,D). The co-diffusion biofilm has a lower maximum oxygen concentration, but a higher maximum NH_2OH concentration in comparison to those in the counter-diffusion biofilm.

The Mred (Mox) concentration peaked (bottomed) at a biofilm depth of $\sim 175 \mu\text{m}$ in the co-diffusion biofilm and at a biofilm depth of $\sim 150 \mu\text{m}$ in the counter diffusion biofilm (Fig. 4B,E). The distribution of N_2O production rate matched the predicted Mred stratification of the biofilm with major contribution from AOB denitrification pathway in both diffusion geometries (Fig. 4C,F). However, the maximum N_2O production rate ($\sim 45 \text{ mg N/L/hour}$) in the co-diffusion biofilm was substantially higher than the one ($\sim 29 \text{ mg N/L/hour}$) in the counter-diffusion biofilm.

Analysis of N_2O production within the co- and counter- diffusion nitrifying biofilms at high oxygen loading ($5.5 \text{ m}^3/\text{d}$). Figure 5 shows the distribution profiles of O_2 , NH_2OH , Mox , Mred and N_2O production rate via the two known pathways within the biofilm, with an influent ammonium concentration of 500 mg N/L, HRT of 12 hours and oxygen supply of $5.5 \text{ m}^3/\text{d}$. Almost all of the influent ammonium were converted to nitrite under the high oxygen loading conditions (Figure S2).

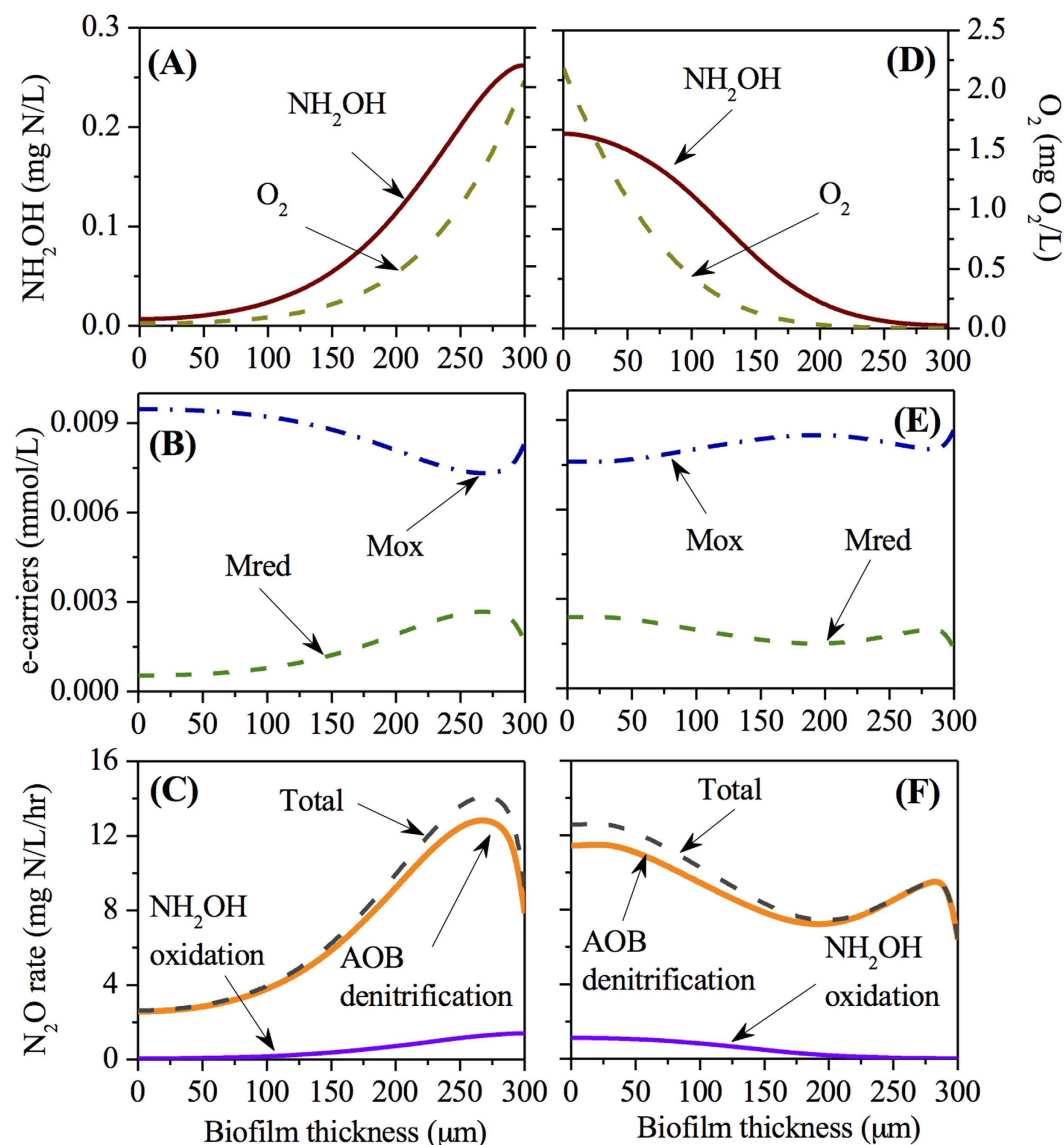


Figure 5. The depth profiles of NH_2OH , O_2 , Mred , Mox and N_2O production rates at high oxygen loading ($5.5 \text{ m}^3/\text{d}$) within the co-diffusion biofilm (A–C) and counter-diffusion biofilm (D–F).

The trend of O_2 and NH_2OH concentration against biofilm depth in both co- and counter-diffusion biofilms were in line with those at lower oxygen loadings in Figs 3 and 4 (Fig. 5A,D). The oxygen was exhausted at $\sim 60 \mu\text{m}$ in the co-diffusion biofilm and at $\sim 190 \mu\text{m}$ in the counter-diffusion biofilm (Fig. 5A–D). The NH_2OH concentration was exhausted at the base of the co-diffusion biofilm and at a biofilm depth of $275 \mu\text{m}$ in the counter-diffusion biofilm.

The Mred (Mox) concentration peaked (/bottomed) at a biofilm depth of $\sim 275 \mu\text{m}$ in the co-diffusion biofilm (Fig. 5B,E). However, there were two highest points for Mred within the counter-diffusion biofilm: one at the base of biofilm and the other at the biofilm depth of $\sim 290 \mu\text{m}$, adjacent to the surface of biofilm. The biofilm distribution of Mred shaped the N_2O production rate within the two types of biofilms (Fig. 5C,F). The AOB denitrification pathway was the main contributor throughout the biofilm, whereas a small contribution of the NH_2OH oxidation pathway to N_2O production occurred at the surface of the co-diffusion biofilm and at the base of the counter-diffusion biofilm.

Model validation using experimental data. The proposed biofilm N_2O model was tested using experimental data from a sequencing batch biofilm reactor (SBBR) performing partial nitrification²⁰. The SBBR had a working volume of 6 L with plastic bio-carriers to facilitate biofilm formation. In each 12-h cycle, 3 L of synthetic wastewater containing 500 mg N/L of ammonium was fed into the reactor, resulting a hydraulic retention time of 24 hour. Off-gas N_2O was collected in gas sampling bags at intervals of 30 min and analyzed by a gas chromatography. The experimental results of N_2O emission from a typical cycle at steady state were used for model evaluation (Fig. 6). Intermittent aeration was applied and thus DO level in bulk liquid ranged from 0 to $1.5 \text{ mg O}_2/\text{L}$ for

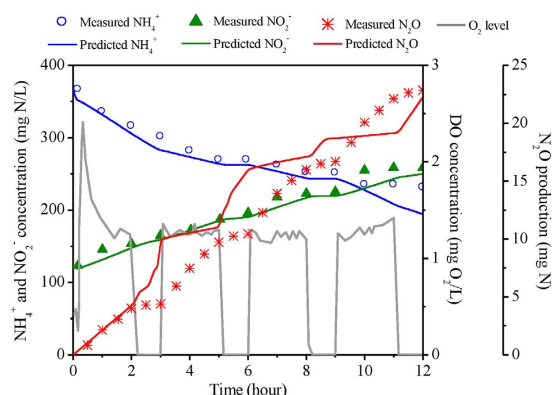


Figure 6. Comparison between model predictions and experimental data from a partial nitrification SBBR.

most cases. NH_4^+ concentration decreased from ~ 370 mg N/L to ~ 230 mg N/L, while NO_2^- accumulated from ~ 120 mg N/L to ~ 260 mg N/L. The total emitted N_2O in this cycle from SBBR is around 22 mg N, leading to an emission factor (defined by the ratio of emitted N- N_2O and N- NH_4^+ loading) of 1.36%. The biofilm N_2O model could satisfactorily capture the dynamics in terms of nitrogen conversions and N_2O production (Fig. 6). The predicted N_2O emission factor was around 1.3%, which well matched the measured value. The good agreement between model predictions and experimental data verified the validity and applicability of the N_2O model for describing N_2O production in nitrifying biofilm systems.

Discussion

Although N_2O production in suspended-growth sludge systems was extensively studied, little effort has been dedicated to investigating N_2O production in biofilm systems, which are of growing significance during wastewater treatment. One of the biggest differences between the complete mixed compartment and the biofilm compartment is that the diffusion of substrates within the biofilm will result in stratified variations of the substrate concentrations. It is known that N_2O would be affected by the precursors of ammonia oxidation^{9,11,17}. With the development of MABR system, the variation of N_2O between the conventional co-diffusion biofilm and the novel counter-diffusion biofilm is also expected due to the changed substrate distribution. A systematic experimental evaluation would take extremely a long time since each process condition would have to be tested for 6–12 months to be representative (when the biofilm system reaches steady state). This is likely the reason why not much data had been produced experimentally to date on such systems. Under such circumstances, this work used a previously-proposed and validated N_2O model incorporating both AOB denitrification pathway and NH_2OH oxidation pathway to give first insights into the difference of N_2O productions from the co- and counter-diffusion biofilm systems.

Our results demonstrate that the stratified oxygen and NH_2OH concentrations within the biofilm affect the N_2O productions via AOB denitrification pathway and hydroxylamine oxidation pathway differently. For both diffusion geometries (Figs 3–5), AOB denitrification pathway is dominant over NH_2OH oxidation pathway within the biofilm under the conditions of varying biofilm depths and oxygen loadings, which is consistent with the observations in a sequencing batch biofilm reactor²⁰ as well as in growth-suspended nitrifying sludges^{7,13}. A small contribution (less than 10%) of NH_2OH oxidation pathway to total N_2O production is observed at the outer layer of the co-diffusion biofilm and at the inner layer of the counter-diffusion biofilm, where the oxygen is more available. Its fraction decreases almost linearly upon the gradual depletion of oxygen through the biofilm (Figs 3–5), suggesting that oxygen may govern the N_2O production via NH_2OH oxidation pathway by regulating the electron supply.¹³ The AOB denitrification pathway in both co- and counter-diffusion biofilms is largely stimulated by the diffusion of NH_2OH into the anoxic region of the biofilm, where no oxygen would compete for the electrons generated by NH_2OH oxidation with NO_2^- (Figs 3–5). High N_2O production rates in the presence of NH_2OH and NO_2^- were also observed under anoxic conditions using suspended cultures^{21,22}. The thicker biofilm generates higher N_2O production is partly due to the extensive anoxic region for nitrite reduction (Fig. 2).

The simulation results indicate that the N_2O production from co-diffusion biofilm is substantially higher than that from counter-diffusion biofilm at thick biofilm (300 μm) in the oxygen loading range of ~ 1 – ~ 4 m^3/d and for other oxygen loadings the two have comparable effluent N_2O concentrations (Fig. 2). This observation is attributed to the effect of co-diffusion and counter-diffusion geometry on substrate distribution. At low oxygen loading (0.24 m^3/d), the distribution profiles of O_2 , NH_2OH , Mred, Mox and N_2O production rate via the two pathways in the co- and counter-diffusion biofilm are approximately mirror-symmetrical, leading to similar effluent N_2O concentration (Fig. 3). However, at moderate oxygen loading (2.4 m^3/d), the depth profiles of O_2 and NH_2OH are quite different in the two diffusion geometries. The co-diffusion biofilm involves a higher NH_2OH concentration and lower O_2 concentration at the surface of biofilm comparing to those at the base of the counter-diffusion biofilm (Fig. 4A,D). Consequently, the anoxic region with the presence of NH_2OH and NO_2^- in co-diffusion is more extended than that in counter-diffusion biofilm, causing a higher peak of Mred and thus a higher N_2O production from nitrite reduction (Fig. 4). By comparing the diffusion of NH_2OH and oxygen within biofilm in Fig. 5A,D, it is seen that i) there is ~ 50 μm of anoxic region in co-diffusion biofilm (Fig. 5A), whereas the anoxic region in

counter-diffusion biofilm is around 100 μm ; ii) the NH_2OH accumulation in anoxic region in co-diffusion biofilm is lower than that in counter-diffusion biofilm. Hence, for high oxygen loading ($5.5 \text{ m}^3/\text{d}$), N_2O production from co-diffusion biofilm is slightly lower than that from counter-diffusion biofilm (Fig. 2C) due to the shrunken anoxic region with lower build-up of NH_2OH in the co-diffusion biofilm.

The biofilm system with the combination of partial nitrification and Anammox has been widely studied and applied in treating digester liquor due to its zero requirement for organic carbon supplement, low sludge yield and low aeration energy consumption^{23–26}. The two geometries of AOB biofilms, evaluated in this study, could be considered as the partial nitrification system producing nitrite for Anammox bacteria. A lower oxygen supply may hamper the autotrophic nitrogen removal efficiency owing to the insufficient nitrite for Anammox (Figure S2). A high oxygen supply (oxygen concentration $> 1.0 \text{ mg O}_2/\text{L}$) could exert an inhibitory effect on Anammox bacteria²⁶. At moderate oxygen loading of $2.4 \text{ m}^3/\text{d}$, both co- and counter-diffusion biofilms are able to provide a effluent $\text{NO}_2^-/\text{NH}_4^+$ ratio of 1.16 (Figure S2), which is very close to the theoretical stoichiometry for Anammox (1.32)²⁷. Under such conditions, the counter-diffusion biofilm (e.g. MABR) should be preferably applied, rather than the conventional co-diffusion biofilm to reduce the N_2O emissions from the system based on the simulation results of this study (Fig. 2). And for both co and counter-diffusion biofilm systems, the simulation results predict a lower N_2O production at thinner biofilm thickness and lower bulk oxygen level (Fig. 2A) due to shrunken anoxic region and a decrease of NH_2OH accumulation within the biofilm. Hence, a proper control of biofilm thickness by shear force and oxygen loading by aeration would help to mitigate N_2O emission from such biofilm systems.

We further tested the biofilm model with low-strength ammonium in the influent (80 mg N/L), HRT of 6 hours and biofilm thickness of $300 \mu\text{m}$. Figure S3 shows the effluent N_2O concentration from co-diffusion and counter-diffusion biofilms under varying oxygen loadings. It is revealed that N_2O productions from the co- and counter-diffusion biofilms are comparable to each other. The co-diffusion biofilm produces a little higher N_2O at oxygen loading rate of around $1 \text{ m}^3/\text{d}$, while counter-diffusion biofilm generates a slightly more N_2O at oxygen loading of approximately $2 \text{ m}^3/\text{d}$. Hence, for treating low-strength ammonium, N_2O production is negligibly influenced by the diffusion geometry of the biofilm.

In order to fully clarify the interactions among N_2O production, NH_2OH and oxygen diffusion, and electron transportation by AOB in biofilms, the simulations in this work are performed based on the assumption that AOB are evenly distributed throughout the biofilm. It has been reported that AOB are able to grow on NH_2OH oxidation and thus occupy an extended biofilm region^{21,28}, while NOB are inhibited in the presence of NH_2OH ^{29,30}. Nevertheless, further investigation is required to reveal the effect of diffusion geometry on N_2O formation in more complex biofilms, where AOB, NOB, Anammox bacteria and/or heterotrophic organisms may co-exist and compete for substrates and growth space within the biofilm.

The model predictions of this work remain to be verified. However, the preliminary results will already support reactor operations under both steady-state and dynamic conditions. For instance, the simulation results can be used for process evaluation and directing pilot-plant research on application of membrane technology with special attention on N_2O production. There is no doubt that the simulation-based observations are subject to further improvement, but the presented findings will serve as an excellent basis for future system development and optimization.

In summary, a previously established and validated two-pathway N_2O model incorporating both AOB denitrification pathway and NH_2OH oxidation pathway is used to assess the effect of co- and counter-diffusion on N_2O production in nitrifying biofilms. AOB denitrification pathway is dominant over NH_2OH oxidation pathway within the co- and counter-diffusion biofilms. The diffusion of NH_2OH and oxygen within the biofilms forming anoxic layers with the presence of NH_2OH and NO_2^- result in a high N_2O production rate via AOB denitrification pathway. The co-diffusion biofilm may generate substantially higher N_2O than the counter-diffusion biofilm due to the higher accumulation of NH_2OH in co-diffusion biofilm, especially under the condition of high-strength ammonium influent (e.g., 500 mg N/L), thick biofilm depth (e.g., $300 \mu\text{m}$) and moderate oxygen loading (e.g., $\sim 1\text{--}4 \text{ m}^3/\text{d}$). The effect of co- and counter-diffusion on N_2O production and the related pathways from the nitrifying biofilms is minimal when treating low-strength nitrogenous wastewater (e.g., 80 mg N/L).

Materials and Methods

The co- and counter- diffusion biofilm reactor model. A one-dimensional AOB biofilm is constructed based on the assumption of a fixed biofilm thickness without any biomass growth, attachment or detachment and a uniform distribution of AOB throughout the biofilm for all cases, using software AQUASIM V2.1³¹. As shown in Fig. 1, the co-diffusion and counter-diffusion biofilm geometries are compared in the model: in the co-diffusion biofilm both oxygen and ammonium (NH_4^+) are supplied into the biofilm from the bulk liquid, whereas in the counter diffusion biofilm, the oxygen and NH_4^+ are dividedly provided to the biofilm base through a gas-permeable membrane and surface of the biofilm from the bulk liquid, respectively (Fig. 1). The biofilm reactor is modeled through consisting of a completely mixed gas compartment and a biofilm compartment (containing biofilm and bulk liquid). The gas compartment is linked to the bulk liquid in the co-diffusion biofilm and connected to the base of biofilm in the counter-diffusion biofilm through diffusive links. The oxygen concentration in the gas compartment is dependent on the gas flow rate and the applied gas pressure. The following kinetics (Equation 1) is used to model the flux of oxygen (Flux_{O_2}) from the gas to the biofilm matrix compartment through the membrane in both biofilm reactors:

$$\text{Flux}_{\text{O}_2} = k_{\text{O}_2} \left(\frac{S_{\text{O}_2, \text{g}}}{H_{\text{O}_2}} - S_{\text{O}_2} \right) \quad (1)$$

where $So_{2,g}$ and So_2 are the concentrations of oxygen in the gas and biofilm matrix compartments (g m^{-3}), respectively, Ko_2 is the overall mass transfer coefficient of oxygen (0.312 m d^{-1})¹⁸ and Ho_2 is the Henry coefficient for oxygen ($\text{mole O}_2 \text{ m}^{-3} \text{ gas/mole O}_2 \text{ m}^{-3} \text{ liquid}$).

The biofilm specific surface area is set at $125 \text{ m}^2/\text{m}^3$. The biofilm density is $50000 \text{ g COD m}^{-3}$. The water fraction of the biofilm matrix is kept constant at 0.75. Parameters with regard to the mass transfer coefficients for the substrates (e.g. ammonium, nitrite, oxygen etc.) are adopted from Hao *et al.*³². The biofilm model assumes no transportation of mediators due to the fact that the electron carriers are immobilized in the stationary microbial phase¹⁷.

The two-pathway N_2O model by AOB. The N_2O model developed and validated by Ni *et al.*¹⁵ integrated both AOB denitrification pathway and NH_2OH oxidation pathway and synthesized relevant biochemical reactions in conversion of ammonia (NH_3), NH_2OH , NO_2^- , NO , N_2O and O_2 . The electron transfer from oxidation to reduction was modeled by introducing electron mediators (Mred and Mox) as the new state variables. The definition and unit for these substrates are presented in Table S1 in Supplementary Material. The kinetics and stoichiometry of the model are shown in Table S2.

The N_2O model is composed of seven processes (Table S2). In process 1, the oxidation of NH_3 to NH_2OH is accompanied by oxygen reduction with one O atom inserted into NH_2OH and the other reduced to water (H_2O). The conversion from Mred to Mox donates a pair of electrons to the O atom. Process 2 involves incomplete oxidation of NH_2OH to NO , during which three electrons are generated. In process 3, the produced NO is then oxidized to NO_2^- , where one electron is formed. Mox would accept four electrons and be converted to Mred during oxidation of NH_2OH to NO_2^- . In process 4, the NO that is formed from incomplete NH_2OH oxidation would be reduced to N_2O (NH_2OH oxidation pathway). Process 5 involves O_2 reduction to H_2O . In process 6, N_2O is produced as the end product during nitrite reduction, which is described as a one-step process without NO intermediate to avoid NO and NO_2^- loop (AOB denitrification pathway). The Process 4, 5 and 6, accompanied by the conversion of Mred to Mox, would compete for the electrons generated from NH_2OH oxidation and play important roles in regulating N_2O production by AOB. In process 7, an increase of Mred is balanced by a decrease of Mox and vice versa ($\text{Mred} \rightleftharpoons \text{Mox} + 2\text{e}^- + 2\text{H}^+$), with the total level of electron carriers (C_{tot}) being constant.

Investigating the impacts of co- and counter- diffusion on N_2O production. The N_2O model by AOB used in this work has been evaluated and verified in both suspended-growth sludge systems^{15,16}, and AOB biofilm system¹⁷. Hence we adapt those reported parameter values in literature (Table S3) to assess N_2O production and other substrate conversions in biofilm system. This model-based evaluation approach has been well demonstrated in different microbial systems^{17,32–35}.

The hydraulic retention time (HRT) for the biofilm compartment is set at 12 hours and the influent ammonium concentration is firstly kept constant at 500 mg N/L to investigate N_2O production under high-strength ammonium conditions. Model simulations are then performed under varying conditions (biofilm thickness from $100\text{--}300 \mu\text{m}$ and oxygen loading rate from $0.24\text{--}5.5 \text{ m}^3/\text{d}$) to provide insight into the effects of co- and counter diffusion on N_2O production from the AOB biofilm. The underlying mechanisms are analyzed with the produced depth profiles of substrate concentrations and reaction rates in the co- and counter-diffusion AOB biofilms. Additional simulations at low influent ammonium concentration (80 mg N/L) are also conducted with the detailed results in Supplementary Material.

References

1. Ravishankara, A. R., Daniel, J. S. & Portmann, R. W. Nitrous oxide (N_2O): the dominant ozone-depleting substance emitted in the 21st century. *Science* **326**, 123–125 (2009).
2. IPCC, *Climate Change, The Physical Science Basis. Contribution of Working Group I to the Fifth Assessment Report of the Intergovernmental Panel on Climate Change*. Cambridge University Press, Cambridge, United Kingdom and New York, NY, USA, p. 1535 (2013).
3. Yu, R., Kampschreur, M. J., Loosdrecht, M. C. M. & Chandran, K. Mechanisms and specific directionality of autotrophic nitrous oxide and nitric oxide generation during transient anoxia. *Environmental Science & Technology* **44**, 1313–1319 (2010).
4. Tallec, G., Garnier, J., Billen, G. & Gossailles, M. Nitrous oxide emissions from secondary activated sludge in nitrifying conditions of urban wastewater treatment plants: Effect of oxygenation level. *Water Research* **40**, 2972–2980 (2006).
5. Kampschreur, M. J., Temmink, H., Kleerebezem, R., Jetten, M. S. M. & Van Loosdrecht, M. Nitrous oxide emission during wastewater treatment. *Water Research* **43**, 4093–4103 (2009).
6. Peng, L., Ni, B. J., Ye, L. & Yuan, Z. N_2O production by ammonia oxidizing bacteria in an enriched nitrifying sludge linearly depends on inorganic carbon concentration. *Water Research* **74C**, 58–66 (2015).
7. Kampschreur, M. J. *et al.* Effect of dynamic process conditions on nitrogen oxides emission from a nitrifying culture. *Environmental Science & Technology* **42**, 429–435 (2007).
8. Chandran, K., Stein, L. Y., Klotz, M. G. & van Loosdrecht, M. C. M. Nitrous oxide production by lithotrophic ammonia-oxidizing bacteria and implications for engineered nitrogen-removal systems. *Biochemical Society Transactions* **39**, 1832–1837 (2011).
9. Kim, S. W., Miyahara, M., Fushinobu, S., Wakagi, T. & Shoun, H. Nitrous oxide emission from nitrifying activated sludge dependent on denitrification by ammonia-oxidizing bacteria. *Bioresour. Technology* **101**, 3958–3963 (2010).
10. Law, Y., Ni, B. J., Lant, P. & Yuan, Z. N_2O production rate of an enriched ammonia-oxidising bacteria culture exponentially correlates to its ammonia oxidation rate. *Water Research* **46**, 3409–3419 (2012).
11. Stein, L. Y. Surveying N_2O -producing pathways in bacteria. *Methods in Enzymology* **486**, 131–152 (2011).
12. Peng, L., Ni, B. J., Ye, L. & Yuan, Z. The combined effect of dissolved oxygen and nitrite on N_2O production by ammonia oxidizing bacteria in an enriched nitrifying sludge. *Water Research* **73C**, 29–36 (2015).
13. Peng, L., Ni, B. J., Erler, D., Ye, L. & Yuan, Z. The effect of dissolved oxygen on N_2O production by ammonia-oxidizing bacteria in an enriched nitrifying sludge. *Water Research* **66C**, 12–21 (2014).
14. Ni, B. J., Yuan, Z., Chandran, K., Vanrolleghem, P. A. & Murthy, S. Evaluating four mathematical models for nitrous oxide production by autotrophic ammonia-oxidizing bacteria. *Biotechnology and Bioengineering* **110**, 153–163 (2013).
15. Ni, B. J., Peng, L., Law, Y., Guo, J. & Yuan, Z. Modeling of nitrous oxide production by autotrophic ammonia-oxidizing bacteria with multiple production pathways. *Environmental Science & Technology* **48**, 3916–3924 (2014).

16. Ni, B. J., Pan, Y., van den Akker, B., Ye, L. & Yuan, Z. Full-Scale modeling explaining large spatial variations of nitrous oxide fluxes in a step-feed plug-flow wastewater treatment reactor. *Environmental Science & Technology* **49**, 9176–9184 (2015).
17. Sabba, F., Picioreanu, C., Pérez, J. & Nerenberg, R. Hydroxylamine diffusion can enhance N_2O emissions in nitrifying biofilms: a modeling study. *Environmental Science & Technology* **49**, 1486–1494 (2015).
18. Terada, A., Lackner, S., Tsuneda, S. & Smets, B. F. Redox-stratification controlled biofilm (ReSCoBi) for completely autotrophic nitrogen removal: the effect of co- versus counter-diffusion on reactor performance. *Biotechnology and Bioengineering* **97**, 40–51 (2007).
19. Peng, L., Ni, B., Ye, L. & Yuan, Z. Selection of mathematical models for N_2O production by ammonia oxidizing bacteria under varying dissolved oxygen and nitrite concentrations. *Chemical Engineering Journal* **281**, 661–668 (2015).
20. Kong, Q. *et al.* Partial nitrification and nitrous oxide emission in an intermittently aerated sequencing batch biofilm reactor. *Chemical Engineering Journal* **217**, 435–441 (2013).
21. Böttcher, B. & Koops, H. P. Growth of lithotrophic ammonia-oxidizing bacteria on hydroxylamine. *FEMS Microbiology Letters* **122**, 263–266 (1994).
22. Chandran, K. & Smets, B. F. Biokinetic characterization of the acceleration phase in autotrophic ammonia oxidation. *Water Environment Research: A Research Publication of the Water Environment Federation* **80**, 732–739 (2008).
23. Pellicer-Nàcher, C. *et al.* Sequentially aerated membrane biofilm reactors for autotrophic nitrogen removal: microbial community composition and dynamics. *Microbial Biotechnology* **7**, 32–43 (2014).
24. Pellicer-Nàcher, C. *et al.* Sequential aeration of membrane-aerated biofilm reactors for high-rate autotrophic nitrogen removal: experimental demonstration. *Environmental Science & Technology* **44**, 7628–7634 (2010).
25. Wang, R. *et al.* Nitrification performance and biofilm development of co- and counter-diffusion biofilm reactors: modeling and experimental comparison. *Water Research* **43**, 2699–2709 (2009).
26. Vlaeminck, S. E., De Clippeleir, H. & Verstraete, W. Microbial resource management of one-stage partial nitrification/anammox. *Microbial Biotechnology* **5**, 433–448 (2012).
27. Strous, M., Heijnen, J. J., Kuenen, J. G. & Jetten, M. S. M. The sequencing batch reactor as a powerful tool for the study of slowly growing anaerobic ammonium-oxidizing microorganisms. *Applied Microbiology and Biotechnology* **50**, 589–596 (1998).
28. de Bruijn, P., Van De Graaf, A. A., Jetten, M. S., Robertson, L. A. & Kuenen, J. G. Growth of *Nitrosomonas europaea* on hydroxylamine. *FEMS Microbiology Letters* **125**, 179–184 (1995).
29. Harper, W. F. *et al.* The effect of hydroxylamine on the activity and aggregate structure of autotrophic nitrifying bioreactor cultures. *Biotechnology and Bioengineering* **102**, 714–724 (2009).
30. Noophan, P. L., Figueroa, L. A. & Munakata-Marr, J. Nitrite oxidation inhibition by hydroxylamine: experimental and model evaluation. *Water Science and Technology: A Journal of the International Association on Water Pollution Research* **50**, 295–304 (2004).
31. Reichert, P. AQUASIM 2.0—user manual Swiss Federal Institute for Environmental Science and Technology. Dübendorf, Switzerland (1998).
32. Hao, X., Heijnen, J. J. & van Loosdrecht, M. C. Sensitivity analysis of a biofilm model describing a one-stage completely autotrophic nitrogen removal (CANON) process. *Biotechnology and Bioengineering* **77**, 266–277 (2002).
33. Ni, B. J. & Yuan, Z. A model-based assessment of nitric oxide and nitrous oxide production in membrane-aerated autotrophic nitrogen removal biofilm systems. *Journal of Membrane Science* **428**, 163–171 (2013).
34. Peng, L. *et al.* Biodegradation of pharmaceuticals in membrane aerated biofilm reactor for autotrophic nitrogen removal: A model-based evaluation. *Journal of Membrane Science* **494**, 39–47 (2015).
35. Kong, Q. *et al.* Partial nitrification and nitrous oxide emission in an intermittently aerated sequencing batch biofilm reactor. *Chemical Engineering Journal* **217**, 435–441 (2013).

Acknowledgements

This work was partially supported by the Recruitment Program of Global Experts, the Natural Science Foundation of China (No. 51578391) and the Foundation of State Key Laboratory of Pollution Control and Resource Reuse (Tongji University), China (No. PCRRY15011).

Author Contributions

L.P., X.D. and B.-J.N. wrote the manuscript and developed the methodology; L.P., J.S. and Y.L. performed data analysis and prepared all figures. All authors reviewed the manuscript.

Additional Information

Supplementary information accompanies this paper at <http://www.nature.com/srep>

Competing financial interests: The authors declare no competing financial interests.

How to cite this article: Peng, L. *et al.* Nitrous Oxide Production in Co- Versus Counter-Diffusion Nitrifying Biofilms. *Sci. Rep.* **6**, 28880; doi: 10.1038/srep28880 (2016).



This work is licensed under a Creative Commons Attribution 4.0 International License. The images or other third party material in this article are included in the article's Creative Commons license, unless indicated otherwise in the credit line; if the material is not included under the Creative Commons license, users will need to obtain permission from the license holder to reproduce the material. To view a copy of this license, visit <http://creativecommons.org/licenses/by/4.0/>